Design of an optofluidic biosensor using the slow-light effect in photonic crystal structures

F. Hosseinibalam,[1,*] S. Hassanzadeh,[1] A. Ebnali-Heidari,[1] and C. Karnutsch[2]

[1]Physics Department, University of Isfahan, Isfahan 81746, Iran

[2]University of Applied Sciences Karlsruhe, Department of Electrical Engineering and Information Technology, Karlsruhe, Germany

*Corresponding author: fhb@sci.ui.ac.ir

Received 21 June 2011; revised 31 August 2011; accepted 19 October 2011; posted 15 November 2011 (Doc. ID 149572); published 7 February 2012

The authors propose a biosensor architecture based on the selective infiltration of photonic crystal (PhC) structures. The proposed sensor consists of a ring cavity coupled to an optofluidic slow-light waveguide in a PhC platform. A high potential sensitivity of 293 nm/refractive index unit is numerically demonstrated, while maintaining an ultracompact footprint. © 2012 Optical Society of America

OCIS codes: 230.5298, 350.4238, 220.4241, 190.4390.

1. Introduction

Optical biosensors, which provide detection and quantification of biological analytes, have emerged as a field of great interest because of the tremendous needs in medical diagnosis, pharmaceuticals, homeland security, food quality control, and environmental testing. An optical biosensor uses an optical transducer that can convert a biorecognition event into a detectable signal. There are two basic detection methods in optical biosensors: fluorescence-based detection and label-free detection [1].

In fluorescence-based detection, a biorecognition element carrying a fluorescent tag is usually utilized to identify the presence of the target molecules. Fluorescence-based detection is highly sensitive, enabling detection limits down to a single molecule. But, it suffers from some drawbacks. Fluorescent detection techniques require additional labeling steps beyond the isolation of the target analyte, which implies additional time, complexity, and reagent costs.

In contrast, in label-free detection, target molecules are detected in their natural forms without any modifications, thus enabling easier and cheaper biodetection. As a result, label-free detection with comparable sensitivity to a fluorescent measurement is highly desirable in the development of state-of-the-art biosensors. Most label-free optical biosensors belong to the category of evanescent-wave sensors [1], in which the evanescent field exponentially decays into the surrounding medium for tens to a few hundreds of nanometers away from the solid sensor surface. These sensors usually utilize the refractive index (RI) change induced by the molecular interaction with the evanescent field as the sensing mechanism. RI change is related to the sample concentration rather than the total sample mass. Therefore, in principle, an RI-based sensor can perform sensitive detection with small sample volumes. Hence, for these biosensors, the ability to detect small RI changes is crucial.

In recent years, there has been a growing interest in planar photonic crystal (PhC) waveguides [2–4] and PhC cavities in the context of label-free biosensors [5]. PhCs are periodic nanostructures in which the dielectric constant varies periodically across the device. PhCs display a wide range of phenomena, such as photonic bandgap effects, the creation of slow or stationary modes, and anomalous refraction and propagation effects [6,7].

To create a PhC cavity, a point defect is introduced in periodic hole nanostructures [8]. PhC-cavity-based

1559-128X/12/050568-09$15.00/0

devices have been presented as biosensors [8,9]. Although PhC cavity structures show promising performance in terms of light confinement, in practical applications, the precise fabrication of a cavity with the exact designed resonance is challenging [2,10]. In addition, mass fabrication of PhC cavity biosensors with identical parameters will pose an enormous challenge. In PhC waveguides, the edge of the mode gap has been used for RI measurements or protein detection. This mode edge is less sensitive to the change in air hole radius than a PhC cavity. For optical label-free biosensors based on PhCs, light–matter interaction significantly influences their sensitivity and detection limit. Recently, planar PhC waveguides in the slow-light regime have been reported experimentally for RI detection and label-free detection by using band-edge effects [11]. In the context of label-free biosensors, slow light holds the promise for further enhancing the light–matter interaction. However, the main issue in sensor design based on PhCs is that all reports that include slow light, i.e., light with an ultralow group velocity, are based on dispersive PhC waveguide designs [6,7,11,12]. Such structures exhibit a resonance near their band-edge frequency, where the group velocity is near zero. The band edge is not the best operating point. First, the dispersion curve near the band edge is typically parabolic, which means that the group velocity changes rapidly with frequency. Second, the band edge presents a cutoff point, where the mode turns from propagation to evanescence. As a result, the slow mode near the band edge appears to be very lossy [13,14]. Both these concerns can be addressed by engineering the dispersion curve of the defect. The broadband slow-light regime refers to a waveguide mode with low group velocity or high group index with only small variation inside the spectral range, which results in low group velocity dispersion (GVD). One challenge in using dispersive PhC waveguides as optical sensors in the slow-light regime is that their large GVD is highly undesirable, as it reduces the peak intensity of pulses through temporal broadening, effectively compromising the light–matter interaction afforded by slow-light spatial pulse compression [13].

In this study, we propose combining an optofluidic low dispersion slow-light waveguide with a ring cavity, infiltrated with analyte. We use low dispersion optofluidic slow-light PhC waveguide structures to yield both low group velocity and low dispersion over a large bandwidth, thereby enabling us to design an ultracompact, low power, and highly sensitive biosensor. The sensing part of the proposed biosensor is created by an optical PhC ring cavity. Photonic crystal ring cavities provide strong confinement of light due to their low bending losses [15]. The parameters of the PhC ring are chosen such that the spectral dip (which is created by the cavity coupling to the waveguide) appears in the slow-light low dispersion region.

The remainder of this paper is organized as follows. In Section 2, we design low dispersion slow-light PhCs by using the plane-wave expansion method. In Section 3, we propose biosensor structures and we study and compare the effects of low dispersion slow light on sensor sensitivity using finite-difference time-domain (FDTD) calculations. Finally, we conclude the paper in Section 4.

2. Sensor Structure

A. Designing Slow-Light-Based Biosensors

As mentioned in Section 1, slow light can enhance light–matter interaction and, hence, the sensing effect. Slow-light enhancement of sensing effects is, however, often hard to take advantage of due to various challenges. For instance, coupling energy into slow-light modes has posed some difficulties, which have been addressed recently [16,17]. Another significant challenge has been the inherently high GVD associated with common approaches to producing slow light in PhCs [18,19]. Recently, the flexibility of the PhC geometry has been exploited to create slow-light modes with little to no dispersion [20,21].

Most of these approaches rely on nanometer-scale engineering of the PhC lattice geometry and, therefore, depend largely on the fabrication process. Recently, it has been suggested to use an optofluidic approach for dispersion engineering and creation of slow light, which should be more robust against fabrication inaccuracies [22].

In this paper, an optofluidic slow-light W1 PhC waveguide is created by fluid infiltration into selected air holes of a standard W1 PhC waveguide (for further details, refer to [22]). A W1 waveguide is created by removing the central row of holes along the propagating direction (Γ–K direction) in an otherwise homogeneous two-dimensional planar PhC [see Fig. 1(a)]. This waveguide sustains a guided mode inside the photonic bandgap and exhibits slow light at the band edge where the dispersion relation has a parabolic form. A triangular PhC lattice that consists of air holes with a periodicity of $a = 410$ nm and a radius of 123 nm ($0.3a$) has been used in our calculations. We restrict our calculations to TE-polarization states, i.e., with the electric field being parallel to the plane of the slab, and assume the effective index of the silicon slab is equal to 2.83.

Figure 1(a) shows a schematic representation of a supercell of an optofluidic W1 PhC waveguide for the creation of dispersionless slow light. The first two rows of air holes (red circles) on either side of the waveguide are infiltrated with a liquid (blue circles). Figure 1(b) displays the calculated TE-polarization band structures of a conventional W1 PhC waveguide (blue dots) and an optofluidic W1 PhC waveguide ($n = 1.5$, red dots). We observe that the fundamental mode dispersion of an optofluidic waveguide exhibits a nearly constant slope between $0.36 < k_z < 0.47$. Figure 1(c) shows the calculated group index n_g for a conventional (blue crosses) and an optofluidic W1 PhC waveguide (red dots). Figure 1(c) illustrates that, unlike a conventional

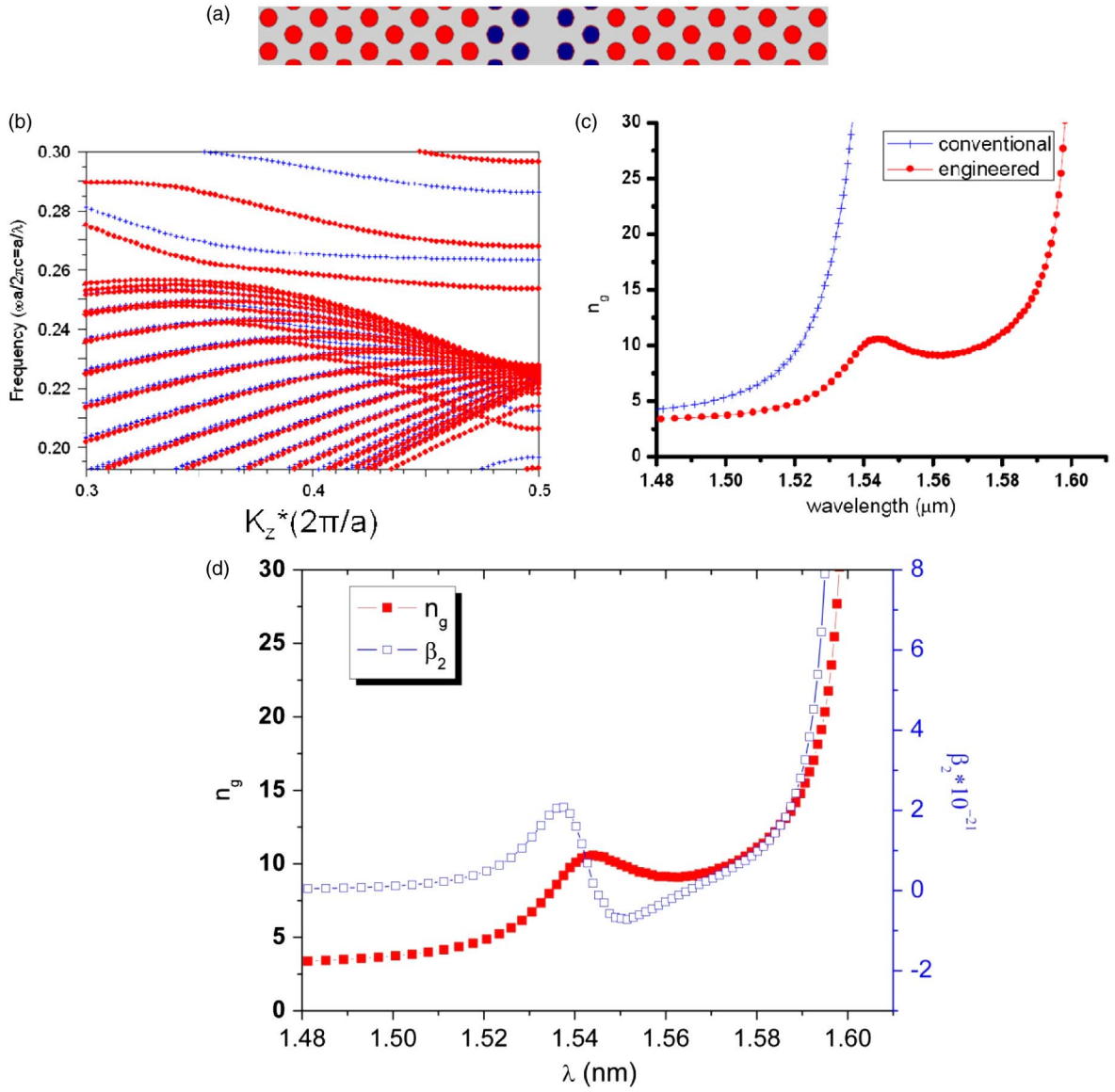

Fig. 1. (Color online) (a) Schematic representation of a supercell of an optofluidic W1 PhC waveguide for creation of dispersionless slow light. The outer red circles represent air holes and the inner blue circles are liquid-infiltrated holes. (b) TE-polarization band structures of a conventional W1 PhC waveguide (blue crosses) and an optofluidic W1 PhC waveguide ($n_{\text{Liquid}} = 1.5$, red dots). (c) Calculated group index for a conventional (blue crosses) and an optofluidic W1 PhC waveguide (red dots). (d) Calculated group index n_g and GVD β_2 for the fundamental mode of an optofluidic W1 PhC waveguide.

W1 PhC waveguide (no infiltrated holes), the optofluidic W1 PhC waveguide typically exhibits a spectral region (here between 1550 and 1590 nm) where the group index is $n_g \approx 10$ and roughly constant over a bandwidth that can be as large as 40 nm. This spectral region is referred to as "low dispersion slow light" [6,7]. In addition, we have calculated the GVD, β_2, of the fundamental mode sustained by a low dispersion optofluidic slow-light PhC waveguide [Fig. 1(d)]. The group index is determined by

$$n_g = n + \omega \frac{dn}{d\omega}. \quad (1)$$

It can be seen that the group index n_g is determined not only by the RI n of the medium but also by the dispersive characteristics of the structure $\omega \cdot dn/d\omega$, where ω is the optical frequency. This dependence can create significant differences between the group velocity (c/n_g) and the phase velocity (c/n), depending on the properties of the medium in which the light propagates. The GVD for a typical optofluidic W1 PhC waveguide is displayed in Fig. 1(d). In the broadband slow-light region (here between 1550 and 1590 nm), where the group velocity has a value of a few percent of the vacuum speed of light, the GVD β_2 has values near zero and is hence negligible.

B. Proposed Biosensor Structure

Our proposed slow-light-based biosensor (SlowBio), which is depicted in Fig. 2(b), is composed of six sections.

(i) Input and output ridge waveguides (sections 1 and 5) to facilitate coupling to the sensor from external optical fibers.
(ii) Coupling sections (sections 2 and 4). Coupling light into a W1 PhC waveguide from input and output ridge waveguides is difficult. To enhance the coupling efficiency, the method of tapering the periodicity of the lattice in the Γ–K direction is used [14,15,19]. The lattice period of the tapered PhC section is linearly decreased from 480 (ridge side) to 410 nm (slow-light side). The length of the coupler section is seven periods.
(iii) Slow-light waveguide (section 3).
(iv) Ring cavity coupled to the W1 waveguide (section 6). This is the sensing region, with the analyte being infiltrated into the yellow-marked holes. The radii and position of the ring cavity are chosen such that the cavity resonant frequencies lie within the slow-light spectral region of the waveguide. The sensing mechanism is based on the wavelength shift of the cavity resonance associated with the RI change induced by the biological sample. In biochemical applications, this change is usually small [e.g., change in RI of 10^{-3}–10^{-4} refractive index unit (RIU)], requiring a large sensor sensitivity. The sensitivity S, given by the ratio of the wavelength shift to the RI change, is proportional to the energy fraction f of the resonant mode field that interacts with the sample (n_f) and, thus, it is natural to maximize the fraction f. The fraction of the resonant mode field that interacts with the sample is calculated using first-order approximation theory [12]:

$$f = \frac{n_f}{\lambda} \times \frac{\Delta\lambda}{\Delta n}. \tag{2}$$

To link the slow light to sensitivity and demonstrate the sensitivity enhancement due to the slow light, we start with the density of states equation, which is given by

$$\rho(\omega) = \frac{1}{(2\pi)^2} \int_S \frac{\mathrm{d}s}{|\nabla \omega_n(k)_n|_{\omega=\omega_n(k)}}. \tag{3}$$

When the integration is carried out over a surface S with constant frequency, $v_g = \nabla\omega(k)$ is the group velocity being inversely proportional to the projected density. Equation (3) gives an explicit relation between the photonic density of states and the band structure of the PhC. In our design, in the slow-light region, the resonance frequency of the ring cavity mode, ω, appears in the low velocity region; consequently, according to Eq. (3), $\rho(\omega)$ assumes a large value. This means that a large number of waveguide states can be coupled to the resonator mode. This is why, due to the slow-light effect, the energy density of the electromagnetic field within the structure, e.g., a biosensor, can be enhanced. This enhances the local fields and increases the light–matter interaction and, thus, f.

Another issue is why we do not work on the band edge. Near the band edge, v_g is zero and van Hove singularity appears in the photonic density of states [23,24]. In other words, the GVD in this region is high. Consequently, the diverging and broadening of electromagnetic modes comes into view. The reason that v_g is related to the strength of the coupling is understood in terms of the density of states of the waveguide modes [25]. In addition, GVD reduces the peak intensity of pulses through temporal broadening, and reduces the f factor. To investigate the performance of the ring cavity only in the flat-band slow-light region, a temporal light pulse is launched into the W1 waveguide. To illustrate that low dispersion slow light can improve sensing, we compare in Fig. 2(c) the calculated transmission spectra of a conventional biosensor (structure depicted in Fig. 2(a)) and a SlowBio sensor for an analyte with $n_f = 1.33$. We observe several spectral dips caused by coupling to the ring cavity. For the SlowBio structure, the spectral dips at $\lambda = 1.56$ and 1.59 μm lie within the low dispersion slow-light regime. As can be seen from Fig. 1(d), in this regime the GVD is negligible and the group index is $n_g \approx 10$. For the SlowBio structure, the transmission of the deepest dip at $\lambda = 1.56$ μm is −13.9 dB, while for the conventional sensor we obtain −1.9 dB at $\lambda = 1.52$ μm. This advantageous behavior is due to the dispersion management and slow-light enhancement. The calculated electric field profile of a SlowBio sensor, when the sensing region is infiltrated with water ($n_f = 1.33$), is shown in Fig. 2(d). As can be seen from Fig. 2(d), light, with maximum efficiency, is coupled from the ridge waveguide to the slow-light region at the cavity resonance wavelength ($\lambda = 1.56$ μm). Such good efficiency is achieved due to the designed coupling sections. In addition, for the resonant wavelength of the ring cavity, shown as a sharp dip in the flat-band slow-light region in Fig. 2(c), the light is coupled to the ring cavity from the slow-light waveguide and trapped inside it. To investigate the strength of the coupling between the slow-light waveguide and the ring cavity, we calculated the steady resonant mode of the ring resonator by assuming a monochromatic light source in CW mode. The assumed wavelength is the same as the resonant wavelength, i.e., the wavelength of the spectral dip in the SlowBio transmission spectrum. Figure 2(d) shows that the electric field is strongly localized in the sensing region and, due to the low-dispersion slow light, light intensity increases; consequently, its interaction with the analyte enhances. In this figure, the darker shade of blue in the cavity region indicates higher field intensity in the cavity region as compared to the electric field in the waveguide region.

Moreover, the sensitivity can be controlled by appropriately choosing the RI of the infiltrated liquid related to the slow light (blue points in the SlowBio), with only a slight penalty in reduction of the slow-light bandwidth. By decreasing the RI of the infiltrated liquid within the slow-light region (blue points), for example $n = 1.45$, we can increase the group index to a value of up to 90. This would

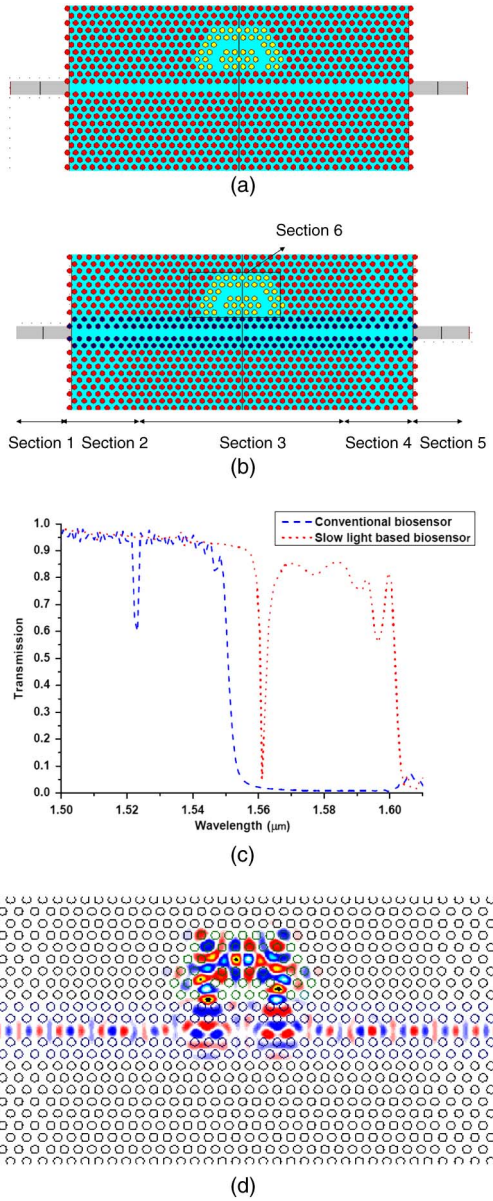

Fig. 2. (Color online) Schematic of the sensor structure for (a) a conventional biosensor and (b) the proposed SlowBio. Sections 1 and 5, ridge waveguide; sections 2 and 4, PhC coupler region; section 6, ring cavity coupled to the W1 waveguide. (c) Transmission spectra for a conventional biosensor (blue dashed curve) and a SlowBio (red dotted curve). (d) Electric field intensity distribution for a slow-light mode coupled to the ring cavity, with the cavity being infiltrated with water ($n_f = 1.33$).

strongly enhance the field overlap f and increase the sensitivity. However, in this case, the slow-light bandwidth would be decreased to 5 nm [22].

C. Sensitivity of the SlowBio Structure

Figure 3 shows the transmission spectra of (a) a SlowBio and (b) a conventional sensor structure when the sensing region is infiltrated with liquids exhibiting different RIs, ranging from $n = 1.33$ (e.g., water) to $n = 1.35$ (e.g., DNA). For the SlowBio structure, in the investigated RI range, all resulting resonances are located within the dispersionless

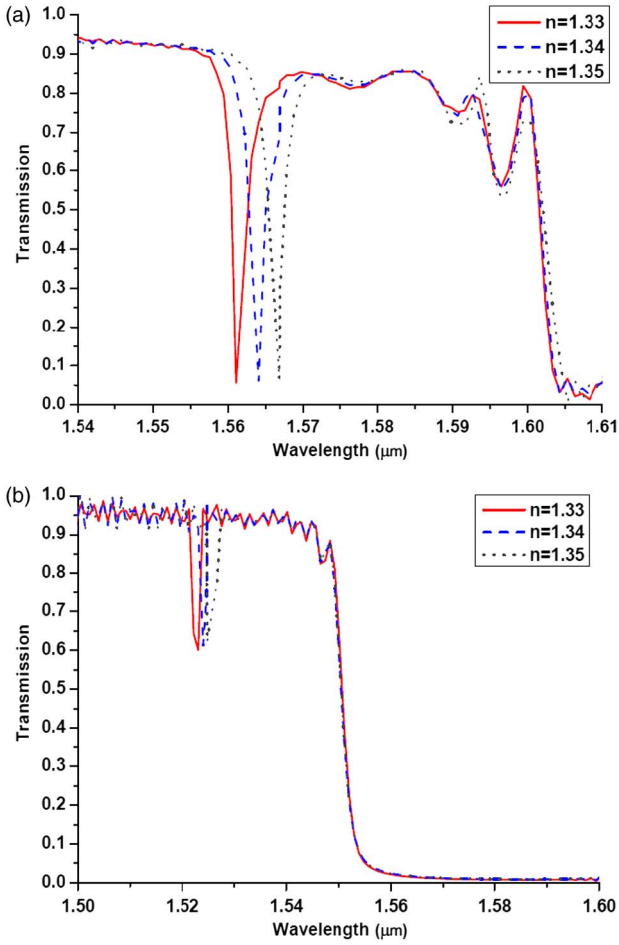

Fig. 3. (Color online) Calculated transmission spectra of (a) the SlowBio and (b) the conventional biosensor, when the ring cavity [yellow-marked holes in Figs. 2(a) and 2(b)] is infiltrated with analytes exhibiting different RIs.

slow-light region. Figure 4 illustrates the calculated sensitivity of the SlowBio and a conventional biosensor. It can be seen that the sensitivity to RI changes is only 77 nm/RIU for the conventional biosensor, but is 293 nm/RIU for the SlowBio. By increasing the RI of the infiltrated liquid within the sensing region, for instance, from $n = 1.48$ to $n = 1.5$, we can see that the resonance wavelength shift is about 6.64 nm, and a sensitivity of 332 nm/RIU for the SlowBio can be achieved. Simulation results reveal that, by infiltrating the sensing region with higher RI, the sensitivity of the SlowBio increases; however, the resonator Q factor decreases. This behavior is observed due to the reduced PhC index contrast [23].

We attribute the larger sensitivity of the SlowBio sensor to the slow-light enhancement. The Q factor of the SlowBio and the conventional biosensor, when the ring cavity is infiltrated with analyte ($n_f = 1.33$), is calculated to be 950 and 650, respectively.

3. Discussion

Our proposed biosensor can be distinguished from previous studies on sensing based on planar PhCs in two main perspectives. First, to the best of our

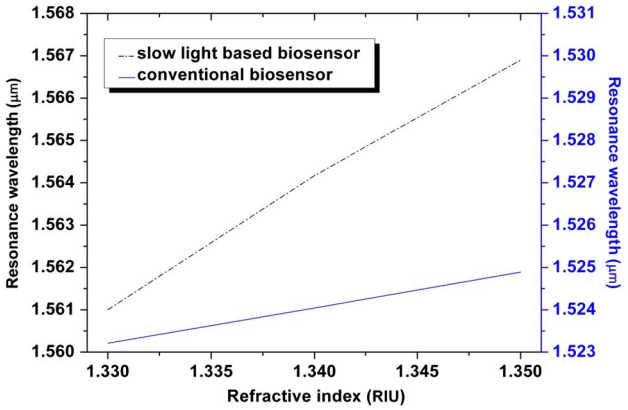

Fig. 4. (Color online) Plot of the resonance wavelength as a function of analyte RI, indicating the sensitivity of the SlowBio to be 293 nm/RIU, and that of the conventional biosensor to be 77 nm/RIU.

knowledge, there is no study including a structure that combines a ring cavity with an optofluidic low dispersion slow-light waveguide. In this study, we have combined an optofluidic low dispersion slow-light waveguide with a ring cavity, into which the analyte is infiltrated, to design a short length (~22 μm), compact (22 μm × 8 μm), and low power (due to the slow light) biosensor. By appropriately designing the biosensor structure, improving the coupling efficiency between the slow-light waveguide and the ring cavity, the guided slow-light mode can be coupled into the ring cavity and sharp spectral dips due to the ring cavity mode frequency appear in the dispersionless slow-light region. This design allows us to detect low-dispersion slow-light dips more easily than the dips located near the band edge of the PhC.

Second, our proposed structure can be used for multipurpose applications. Recently, Monat *et al.* [26] showed how various nonlinear phenomena are enhanced due to slow light in PhC waveguides. Furthermore, they discussed the potential of slow light in PhCs for realizing compact nonlinear devices, operating at low powers. By comparing our work with their study in slow-light designing, it can be found that, by working far away from the ring resonance wavelength, our waveguide, also due to the flat-band slow light, has potential in designing compact, low-power, and all-optical signal processing devices. In addition, by working near the ring resonance wavelength, as we showed, our structure can be used as a biosensor. This advantage, multipurpose applications, is due to the large bandwidth of our designed SlowBio structure.

In the following, the effects of some of the design parameters, such as ring radius, coupling distance, and RI of the analyte, will be discussed. We note that, after performing a series of calculations and examining the results, it is found that the optimum structure to achieve the strongest spectral resonant dip within the slow-light region was the one illustrated in Fig. 2(a). In the optimum structure, the sensing region is a half-ring cavity to avoid any consequential degradation of the low-dispersion slow-light effect (a change in the index of air holes between the waveguide and the cavity results in degradation of the coupling efficiency and the slow-light dispersion) [22].

Another important question is the accuracy of the infiltration method. To answer this question, it has been experimentally proven that high precision and good reproducibility of local filling of tiny PhC holes is achievable by means of selective infiltration techniques. For instance, Erickson *et al.* [27] used an integrated microfluidic circuit, Bog *et al.* [28] took advantage of an actuated microtip, and Smith *et al.* [29] used a micropipette whose size is comparable to the tiny PhC air holes.

Moreover, the transmission spectra are also calculated, when the sensor section area is changed from the two-row ring to a one-row ring [compare Fig. 2(b) and Fig. 5(a)]. Figure 5(a) shows a schematic representation of a SlowBio structure, where the ring cavity consists of only one row of holes. Figures 5(b) and (c) illustrate the transmission spectra and the calculated sensitivity of the SlowBio sensor when the analyte in the sensing region is changed from $n = 1.33$ to $n = 1.35$. In a similar manner to the resonance dip shift in Fig. 3(a), we can see that a shift associated with the relevant materials took place in Fig. 5(b), as well. Figure 5(c) illustrates that the sensitivity to RI changes of the SlowBio sensor with a one-row ring cavity structure is reduced to 187 nm/RIU, as compared to the optimum two-row ring cavity structure with a sensitivity of 293 nm/RIU. Meanwhile, the infiltration of liquids into the SlowBio with two-row holes will, in practice, be easier than the SlowBio with one-row holes. More interesting results were obtained when the calculations of a three-row ring cavity showed that the sensitivity of the SlowBio was stable and equal to that of the optimum two-row structure. But, the infiltration of three-row cavities will be comparably easier than the infiltration into one-row and two-row structures.

About the vertical coupling distance between the slow-light waveguide and the ring cavity, the investigations showed that, because the slow-light interaction is strong with the first two rows of holes, increasing the vertical coupling distance of the ring resonator reduced the slow-light interaction. As a result, due to the resulting weak overlap between light and the infiltrated fluid, the sensitivity of the sensor is very low. Then, the vertical coupling distance started just after the first two rows shown in blue.

In addition, we compare the sensitivity between a resonator-only system, i.e., a ring cavity without the waveguide, and a waveguide–resonator system, i.e., a conventional biosensor. To probe the resonance of the resonator-only system, we carried out FDTD calculations without the waveguide and evaluated the resonance wavelength. For this, a temporal light pulse is launched in the center of the resonator.

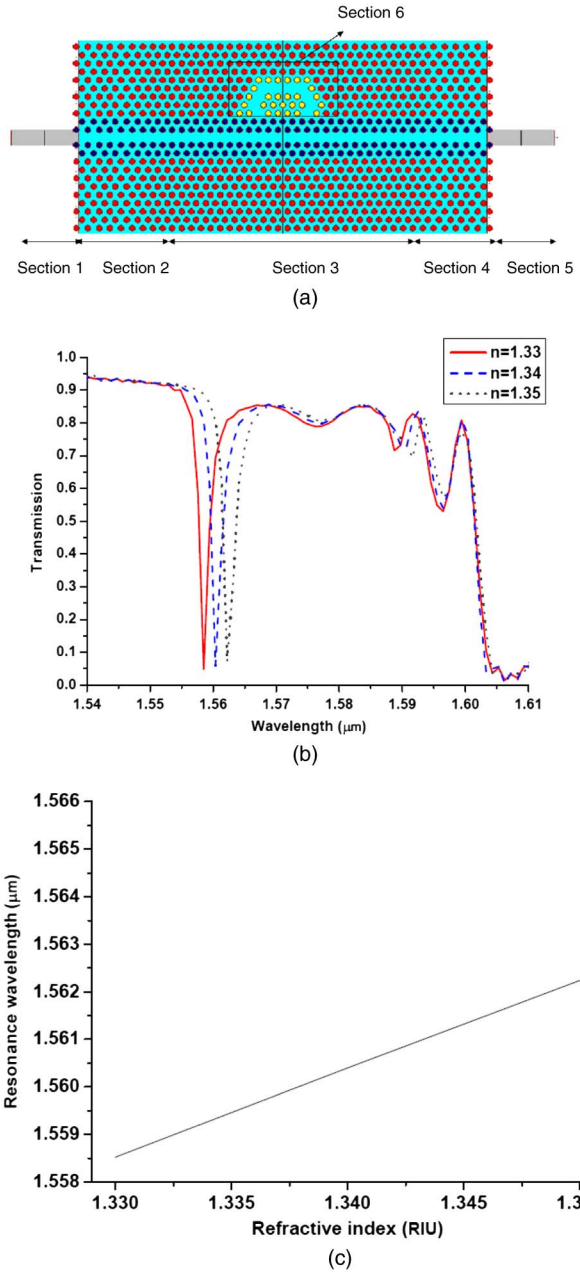

Fig. 5. (Color online) (a) Schematic of the SlowBio structure, where the outer ring of the ring cavity consists of only one row of holes. (b) Transmission spectra of the biosensor when the analyte RI is changed from $n = 1.33$ to $n = 1.35$. (c) Plot of the resonance wavelength as a function of analyte RI, indicating the sensitivity of the SlowBio to be 187 nm/RIU.

The output signal is recorded by a time monitor at the sensing region. Figure 6(a) shows the transmission spectra of the resonator-only system, when the sensing region is infiltrated with liquids exhibiting different RIs ranging between $n = 1.33$ (e.g., water) to $n = 1.35$ (e.g., DNA). Comparing Fig. 6(a) and the blue curve in Fig. 2(c) reveals that the resonance wavelength of the resonator-only system and the conventional biosensor is nearly identical when the sensing region is infiltrated with water ($n = 1.33$). This is because the perturbation due to the introduction of

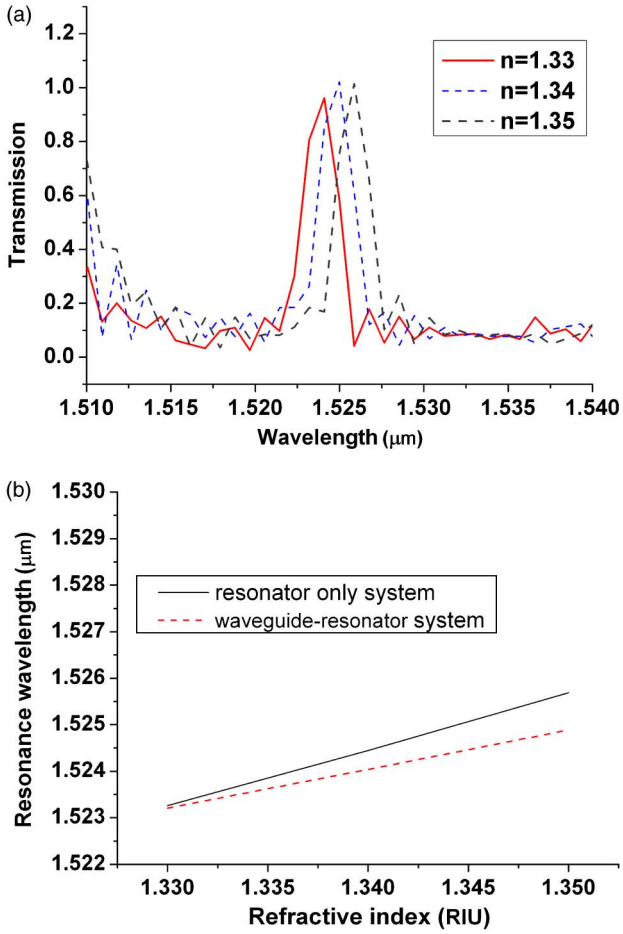

Fig. 6. (Color online) (a) Transmission spectra of a resonator-only system when the sensing region is infiltrated with liquids exhibiting RIs in the range of $n = 1.33$ to $n = 1.35$. (b) Calculated sensitivity of the resonator-only system and the waveguide–resonator system when the sensing region is infiltrated with an RI of $n = 1.33$.

the waveguide is small and, hence, the nature of the resonance is unaltered. But in the SlowBio structure, the perturbation due to the introduction of the optofluidic waveguide is not small. Hence, the resonator properties of the SlowBio structure change. This leads to, by appropriately designing the sensor structure, the resonance wavelength appearing in the flat-band slow-light region. Figure 6(b) compares the calculated sensitivity of the resonator-only system and the waveguide–resonator system, when the sensing region is infiltrated with water ($n = 1.33$). From Fig. 6(b), it can be seen that the sensitivity to RI of the resonator-only system is 100 nm/RIU, while the sensitivity is 77 nm/RIU for the conventional biosensor. This behavior is observed because the resonator-only system experiences larger light–matter interaction than the conventional biosensor, consequently having higher sensitivity. In other words, in the resonator-only system, the losses occur only through the outer border of the PhC, while in a conventional biosensor, losses occur both through the outer border of the PhC and through the waveguide.

In practical applications, the waveguide–resonator system is usually preferred over a resonator-only system due to difficulties in coupling light into the resonator-only system.

Considering the findings of previous studies in this area, it is argued that the sensitivity of the biosensor is improved by using an optofluidic low dispersion slow-light planar PhC waveguide platform. For instance, Garcia *et al.* [11] found that the sensitivity was 178 nm/RIU for planar PhC waveguides working on the shift of the band edge in the slow-light regime. The sensitivity of the SlowBio sensor is higher than most reported results for other planar PhC sensors, such as 70 nm/RIU [30], 103 nm/RIU [31], 212 nm/RIU [5], or 184 nm/RIU [32]. But we note that our reported sensitivity is lower than that found by other studies on slotted PhC waveguides based on a heterostructure cavity [32,33]. However, coupling of light to such structures is much more difficult than the presented structure.

4. Conclusion

A novel SlowBio based on an optofluidic approach is presented. The slow-light part can easily be engineered using selective liquid infiltration. The proposed biosensor is composed of a half-ring cavity that is coupled to an optofluidic slow-light PhC waveguide. In our calculations, the sensitivity to RI changes of the analyte was found to be 293 nm/RIU. This is a promising result for the use of those biosensors in applications such as biochemical and biomedical sensing and diagnosis.

The Iranian authors thank the office of Graduate Studies of the University of Isfahan for their support.

References

1. X. Fan, I. M. White, S. I. Shopoua, H. Y. Zhu, J. D. Suter, and Y. Z. Sun, "Sensitive optical biosensors for unlabeled targets: a review," Anal. Chim. Acta **620**, 8–26 (2008).
2. W. Bogaers, V. Wiaux, P. Dumon, D. Taillaert, J. Wouters, S. Beckx, J. Van Campenhout, B. Luyssaert, D. Van Thourhout, and R. Baets, "Large-scale production techniques for photonic nanostructures," Proc. SPIE **5225**, 101–112 (2003).
3. O. Levi, W. Suh, M. M. Lee, J. Zhang, S. R. J. Brueck, S. Fan, and J. S. Harris, "Guided-resonance in photonic crystal slabs for biosensing applications," in *Conference on Lasers and Electro-Optics/Quantum Electronics and Laser Science Conference and Photonic Applications Systems Technologies*, Technical Digest (CD) (Optical Society of America, 2006), paper CTuK1.
4. M. Askari, S. Yegnanarayanan, and A. Adibi, "Photonic crystal waveguide based sensors," Proc. SPIE **7946**, 794614 (2011).
5. E. Chow, A. Grot, L. W. Mirkarimi, M. Sigalas, and G. Girolami, "Ultracompact biochemical sensor built with two-dimensional photonic crystal microcavity," Opt. Lett. **29**, 1093–1095 (2004).
6. T. F. Krauss, "Why do we need slow light?" Nat. Photon. **2**, 448–450 (2008).
7. T. Baba, "Slow light in photonic crystals," Nat. Photon. **2**, 465–473 (2008).
8. S. John, "Strong localization of photons in certain disordered dielectric superlattices," Phys. Rev. Lett. **58**, 2486–2489 (1987).
9. I. M. White and X. D. Fan, "On the performance quantification of resonance refractive index sensors," Opt. Express **16**, 1020–1028 (2008).
10. N. Skivsen, A. Tetu, M. Kristensen, L. H. Frandsen, and P. I. Borel, "Photonic-crystal waveguide biosensor," Opt. Express **15**, 3169–3176 (2007).
11. J. Garcia-Ruperez, V. Toccafondo, M. J. Banuls, J. G. Castello, A. Griol, S. Peransi-Llopis, and A. Maquierira, "Label-free antibody detection using band edge fringes in SOI planar photonic crystal waveguides in the slow-light slow light regime," Opt. Express **18**, 24276–24286 (2010).
12. N. A. Mortensen, S. Xiao, and J. Pedersen, "Liquid-infiltrated photonic crystals," Microfluid. Nanofluid. **4**, 117 (2008).
13. R. J. P. Engelen, Y. Sugimoto, Y. Watanabe, J. P. Korterik, N. Ikeda, N. F. van Hulst, K. Asakawa, and L. Kuipers, "The effect of higher-order dispersion on slow light propagation in photonic crystal waveguides," Opt. Express **14**, 1658–1672 (2006).
14. L. O'Faolain, T. P. White, D. O'Brien, X. Yuan, M. D. Settle, and T. F. Krauss, "Dependence of extrinsic loss on group velocity in photonic crystal waveguides," Opt. Express **15**, 13129–13138 (2007).
15. V. Kumar, T. Srinivas, and A. Selvarajan, "Investigation of ring resonators in photonic crystal circuits," Photon. Nanostr. Fundam. Appl. **2**, 199–206 (2004).
16. J. P. Hugonin, P. Lalanne, T. P. White, and T. E. Krauss, "Coupling into slow-mode photonic crystal waveguides," Opt. Lett. **32**, 2638–2640 (2007).
17. P. Pottier, M. Gnan, and R. De La Rue, "Efficient coupling into slow-light photonic crystal channel guides using photonic crystal tapers," Opt. Express **15**, 6569–6575 (2007).
18. X. Letartre, C. Seassal, C. Grillet, P. Rojo-Romeo, P. Viktorovitch, M. L. d'Yerville, D. Cassagne, and C. Jouanin, "Group velocity and propagation losses measurement in a single-line photonic-crystal waveguide on InP membranes," Appl. Phys. Lett. **79**, 2312–2314 (2001).
19. M. Notomi, K. Yamada, A. Shinya, J. Takahashi, C. Takahashi, and I. Yokohama, "Extremely large group velocity dispersion of line-defect waveguides in photonic crystal slabs," Phys. Rev. Lett. **87**, 2539021 (2001).
20. J. Li, T. P. White, L. O'Faolain, A. Gomez-Iglesias, and T. F. Krauss, "Systematic design of flat band slow light in photonic crystal waveguides," Opt. Express **16**, 6227–6232 (2008).
21. S. Kubo, D. Mori, and T. Baba, "Low-group-velocity and low-dispersion slow light in photonic crystal waveguides," Opt. Lett. **32**, 2981–2983 (2007).
22. M. Ebnali-Heidari, C. Grillet, C. Monat, and B. J. Eggleton, "Dispersion engineering of slow light photonic crystal waveguides using microfluidic infiltration," Opt. Express **17**, 1628–1635 (2009).
23. G. J. Pedersen, S. S. Xiao, and N. A. Mortensen, "Limits of slow light in photonic crystals," Phys. Rev. B **78**, 153101 (2008).
24. A. A. Krokhin and P. Halevi, "Influence of weak dissipation on photonic band structure of periodic composites," Phys. Rev. B **53**, 1205–1214 (1996).
25. K. Nagahara, M. Morifuji, and M. Kondow, "Optical coupling between a cavity mode and a waveguide in a two-dimensional photonic crystal," Photon. Nanostr. Fundam. Appl. **9**, 261–268 (2011).
26. C. Monat, B. Corcoran, M. Ebnali-Heidari, C. Grillet, B. J. Eggleton, T. P. White, L. O'Faolain, and T. F. Krauss, "Slow light enhancement of nonlinear effects in silicon engineered photonic crystal waveguides," Opt. Express **17**, 2944–2953 (2009).
27. D. Erickson, T. Rockwood, T. Emery, A. Scherer, and D. Psaltis, "Nanofluidic tuning of photonic crystal circuits," Opt. Lett. **31**, 59–61 (2006).
28. U. Bog, C. L. C. Smith, M. W. Lee, S. Tomljenovic-Hanic, C. Grillet, C. Monat, L. O'Faolain, C. Karnutsch, T. F. Krauss, R. C. McPhedran, and B. J. Eggleton, "High-Q microfluidic cavities in silicon-based two-dimensional photonic crystal structures," Opt. Lett. **33**, 2206–2208 (2008).
29. C. L. C. Smith, U. Bog, S. Tomljenovic-Hanic, M. W. Lee, D. K. C. Wu, L. O'Faolain, C. Monat, C. Grillet, T. F. Krauss, C. Karnutsch, R. C. McPhedran, and B. J. Eggleton, "Reconfigurable microfluidic photonic crystal slab cavities," Opt. Express **16**, 15887–15896 (2008).

30. M. R. Lee and P. M. Fauchet, "Nanoscale microcavity sensor for single particle detection," Opt. Lett. **32**, 3284–3286 (2007).
31. D. Dorfner, T. Zabel, T. Hürlimann, N. Hauke, L. Frandsen, U. Rant, G. Abstreiter, and J. Finley, "Photonic crystal nanostructures for optical biosensing applications," Biosens. Bioelectron. **24**, 3688–3692 (2009).
32. S. H. Kwon, T. Sunner, M. Kamp, and A. Forchel, "Optimization of photonic crystal cavity for chemical sensing," Opt. Express **16**, 11709–11717 (2008).
33. A. Di Falco, L. O'Faolain, and T. F. Krauss, "Chemical sensing in slotted photonic crystal heterostructure cavities," Appl. Phys. Lett. **94**, 063503 (2009).